Monte Carlo Simulations of Reaction Kinetics for Ethane Hydrogenolysis over Pt

Simon G. Podkolzin, Rafael Alcala, Juan J. de Pablo, and James A. Dumesic*

Department of Chemical Engineering, University of Wisconsin, Madison, Wisconsin 53706

Received: February 6, 2002; In Final Form: July 17, 2002

A Monte Carlo (MC) molecular model, with parameters derived from density functional theory calculations, is used to describe experimental data for the rate of ethane hydrogenolysis for a Pt/SiO_2 catalyst over a wide range of conditions. The surface concentrations of the most abundant stable species (hydrogen atoms, ethylidyne species, and di-σ-bonded ethylene) are simulated with a MC grandcanonical ensemble, and the rate of ethane hydrogenolysis is calculated by simulating surface concentrations for three types of transition state complexes for C−C bond cleavage. The simulation shows that larger repulsive interactions between adsorbed C_2H_x and H species lead to more negative reaction orders with respect to the hydrogen pressure. The results of the MC simulation indicate that the reaction proceeds primarily through C−C bond cleavage in adsorbed C_2H_5 species, with smaller contributions from adsorbed $CHCH_3$ and $CHCH_2$ species. The MC results suggest that although the most abundant surface hydrocarbon species has a stoichiometry of C_2H_3, the reaction proceeds through more highly hydrogenated C_2H_5 species. The state of the surface is predicted to change from being primarily hydrogen-covered at most experimental conditions to being highly hydrocarbon-covered at low hydrogen partial pressures.

1. Introduction

Monte Carlo (MC) molecular simulations of kinetic processes, with incorporation of results from electronic-structure calculations based on density function theory (DFT), provide an effective means to describe the kinetics of catalytic reactions on surfaces.[1−4] Although the absolute rates of chemical reactions can be simulated with time-dependent MC algorithms,[1] the computational challenge for most systems is to model reaction steps with vastly different time scales. In this paper, we separate the molecular modeling of reactions that occur much faster than the rate of the overall reaction by treating these quasi-equilibrated steps with a classic MC ensemble, rather than with a time-dependent algorithm. Results from Monte Carlo simulations of quasi-equilibrated steps then provide a background for modeling slow reaction steps.

We have previously reported a model, based on a grand-canonical MC ensemble,[5] for the coadsorption of hydrogen atoms and ethylidyne species on Pt(111) from gaseous mixtures of H_2 and ethane at various temperatures and partial pressures. This model is extended in the present paper to provide a description of a quasi-equilibrated background for a Pt catalytic surface under typical ethane hydrogenolysis reaction conditions. In particular, we combine the quasi-equilibrated coadsorption background for abundant surface species on Pt with a model describing the rate-limiting step in ethane hydrogenolysis, i.e., cleavage of the C−C bond in various C_2H_x surface species. All parameters of the combined model (i.e., adsorption energies for surface species and their pairwise lateral interactions) are estimated from results of DFT calculations. In this respect, we complement the DFT results reported earlier[6] on the stability and reactivity of the C_2H_x species and atomic hydrogen on clean Pt surfaces with new DFT calculations on the energetics of pairwise lateral interactions. The combined MC model successfully simulates experimental data for the reaction kinetics of ethane hydrogenolysis[7] for a Pt/SiO_2 catalyst over a wide range of reaction conditions: $P_{H_2} = 3-60$ kPa, $P_{C_2H_6} = 0.7-13$ kPa, 573−673 K.

* Corresponding author. Fax: (608) 262-5434. E-mail: Dumesic@engr.wisc.edu.

2. Background

2.1. Kinetics of Ethane Hydrogenolysis on Pt. Ethane hydrogenolysis is widely used as a probe reaction for studying the catalytic conversion of hydrocarbons on metals. The kinetics of this reaction over Pt have been extensively studied,[7−10] because of the wide use of Pt-containing catalysts in the petroleum and chemical industries. It has been established that C−C bond scission reactions typically have higher activation barriers than those for hydrogenation−dehydrogenation or hydrogen exchange steps.[11−13] For example, the activation energy for the single H/D exchange of deuterated ethylene with hydrogen over Pt was estimated to be approximately 45 kJ/mol. A similar activation energy of 37−46 kJ/mol was reported for ethylene hydrogenation over Pt.[14] These barriers are significantly lower than the activation energy of approximately 200 kJ/mol for ethane hydrogenolysis.[7,10] Furthermore, H/D exchange reactions between ethane and deuterium were found to be 3 orders of magnitude faster at 475−625 K than the rate of ethane hydrogenolysis.[11] Therefore, hydrogen adsorption−desorption steps and various hydrogenation−dehydrogenation steps leading to the formation of adsorbed C_2H_x species from gas-phase ethane on Pt can be treated as quasi-equilibrated processes in ethane hydrogenolysis reaction models. Furthermore, the methane pressure does not influence the rate of ethane hydrogenolysis. Consequently, hydrogenation of C_1 species and methane desorption reaction steps can be treated as fast and irreversible processes.

Based on the above experimental observations, proposed mechanisms for ethane hydrogenolysis over Pt typically have several common features.[7−9,15,16] The reaction steps include quasi-equilibrated, dissociative adsorption of hydrogen and

10.1021/jp020345z CCC: $22.00
Published on Web 08/27/2002

ethane with the formation of atomic hydrogen and various C_2H_x species. The reaction is thought to proceed by C−C bond scission in the most abundant reactive C_2H_x surface species. This slow step is followed by fast hydrogenation of C_1 fragments and methane desorption. These features are summarized schematically in the following reaction scheme, initially proposed by Cimino et al.:[15]

$$C_2H_6 + Pt \rightleftarrows C_2H_x(ads) + \left(\frac{6-x}{2}\right)H_2 \quad (1)$$

$$C_2H_x(ads) + \left(\frac{8-x}{2}\right)H_2 \rightarrow 2\ CH_4 \quad (2)$$

Results of reaction kinetics analyses by Sinfelt et al. suggest that the reaction proceeds via highly dehydrogenated C_2H_x species.[8] Studies by Klug et al. using NMR techniques indicate that adsorbed C_2H_3 surface species may be the most abundant hydrocarbon fragments on the catalyst surface.[17] Reaction kinetics modeling based on De Donder relations with incorporation of DFT results for Pt(111) and Pt(211) suggests that the catalytic surface is covered primarily by nonreactive ethylidyne species, $C-CH_3$, but the reaction proceeds primarily through more highly dehydrogenated species such as adsorbed C_2H_5 and $CH-CH_3$.[16]

2.2. Hydrogen Adsorption on Pt. The dissociative adsorption of hydrogen on Pt becomes quasi-equilibrated at temperatures near 100−180 K, as evidenced by adsorption−desorption, work function, and nuclear microanalysis experiments.[18,19] A low activation energy, 5−9 kJ/mol, has been reported for hydrogen−deuterium exchange on Pt(111) for the temperature range 150−570 K.[20,21] At higher temperatures, the exchange was found to be nonactivated.[21] Results from temperature-programmed desorption studies have been used to estimate the heats of hydrogen adsorption on single-crystal surfaces. The first desorption peak at 150 K (state β_1) can be attributed to weakly adsorbed hydrogen on hcp sites.[22,23] The remaining hydrogen on the fcc sites desorbs in two subsequent peaks at 230 and 300 K (β_2 and β_3) due to a second-neighbor repulsive interactions.[20] The initial heat of adsorption on Pt(111) was found to be in the range from −75 to −85 kJ/mol.[21,23]

Comparisons of the energetics of hydrogen adsorption on Pt(111) terrace sites and on step/edge sites (e.g., a (997) plane) showed that the step/edge sites have heats that are stronger by 12−15 kJ/mol.[20,24,25] In agreement with these results, the initial heats for adsorption of hydrogen on polycrystalline films, filaments, and supported Pt materials, which are expected to have a measurable number of step/edge sites, were found to be about −95 kJ/mol.[26−29] The integral heat of adsorption was reported to be independent of the dispersion for supported Pt.[30] Moreover, the dependence of the differential heat versus coverage was the same on samples with different metal particle sizes.[28] Furthermore, this dependence is similar for a wide variety of Pt surfaces.[26,27,29] Based on this similarity, it is appropriate to choose ideal crystal planes with well-defined and characterized surfaces sites as models for simulating uptake and energetics for hydrogen adsorption on highly dispersed Pt catalysts. For example, our analysis of calorimetric results for supported Pt catalysts with different dispersions indicates that about 90% of surface sites have Pt(111) energetics, and as a result, these sites can be described by a MC model based on an ideal Pt(111) surface.[5]

DFT calculations for adsorption of H atoms on Pt(111) showed that all four high-symmetry sites (i.e., atop, bridge-bonded, fcc and hcp sites) have similar energetics and low diffusion barriers.[31−33] The calculations predict a value for the initial heat of hydrogen adsorption of about −80 kJ/mol, with slightly weaker adsorption at higher coverages.

2.3. Ethane Adsorption on Pt. Spectroscopic studies show that at temperatures above 300 K, ethane adsorbs on Pt dissociatively with the formation of primarily di-σ-bonded ethylene and ethylidyne species.[34,35] Vibrational spectra of these hydrocarbon species are similar to those obtained from ethylene adsorption. The only significant difference on ethane adsorption is the absence of peaks for weakly adsorbed π−bonded ethylene species, which are detected in the presence of gas-phase ethylene. The nature of the most abundant adsorbed C_2 species depends on temperature and partial pressure. For example, in-situ spectroscopic studies during ethylene hydrogenation show that increasing hydrogen pressure shifts the surface coverage toward di-σ-bonded ethylene species compared to adsorbed ethylidyne species.[14,36]

Ethylidyne and di-σ-bonded ethylene species adsorbed on different Pt surfaces have been characterized using various experimental techniques (e.g., refs 37−41). Results from microcalorimetric and infrared spectroscopic studies of ethylene adsorption on Pt powder and silica-supported Pt samples are similar to results reported for Pt(111). Specifically, the heat of adsorption of ethylene to form ethylidyne species and surface hydrogen atoms on Pt(111) was reported by King et al. to be -174 ± 4 kJ/mol,[42] and results from microcalorimetric studies of Pt powder and silica-supported Pt yielded slightly lower values of −145 to −157 kJ/mol.[29,40] Similar values of about −150 kJ/mol were reported for Pt films.[43] The heats of adsorption for di-σ-bonded ethylene on different Pt surfaces are also similar: about −120 kJ/mol on supported Pt and Pt powder samples and −136 kJ/mol on Pt(110)(2 × 1).[40,44,45]

Results from electronic structure calculations have elucidated details of geometries and energetics for ethylidyne and di-σ ethylene surface species.[6,40,46,47] Ethylidyne species adsorb preferentially in 3-fold fcc sites, with the C−C bond orthogonal to the surface and the methyl group pointing away from the surface. Adsorption in the 3-fold hcp site has been found to be only slightly less energetically favorable. Calculations of the energetics for other sites on the (111) plane and interpretations of STM data suggest that ethylidyne species are mobile even at low temperatures.[46] The di-σ-bonded ethylene species adsorb in a bridge site, with the C−C axis parallel to the surface. The C−C and Pt−C bond distances for both species are about 1.5 and 2.1 Å, respectively. Calculated energy changes for ethylene adsorption on Pt(111) at 298 K are equal to −97 kJ/mol for di-σ species and −184 kJ/mol for ethylidyne and hydrogen, and these values are in agreement with results from microcalorimetric measurements.[6]

3. DFT Calculations

The starting point for the MC simulations of the present study is based on the energetics of adsorbed C_2H_x species and atomic hydrogen on Pt(111) and Pt(211) surfaces reported earlier.[6] These energetics are summarized in Table 1. All binding energy calculations were performed with the DACAPO software from the Danish Technical University. In these calculations, two-layer Pt(111) and Pt(211) periodically repeated fixed slabs with a 2 × 2 unit cell were used. Ionic cores were described by ultrasoft pseudopotentials, and the Kohn−Sham one-electron valence states were expanded in a basis of plane waves with kinetic energies below 25 Ry. The surface Brillouin zone was sampled at 18 special *k*-points. The exchange-correlation energy

TABLE 1: Energetics of Reaction Steps, kJ/mol

reaction	ΔU(0K)	ΔH(623K)	ΔU(623K) ΔH(623K) − ΔnRT	ΔU_{model}
(1) $C_2H_6 + Pt(211) \rightarrow C_2H_3{-}Pt + 1.5H_2$	45	17	14	$\Delta_{623K} - 20^a = -6$
(2) $C_2H_6 + Pt(211) \rightarrow C_2H_4(di\text{-}\sigma){-}Pt + H_2$	−1	−18	−18	$\Delta_{623K} - 20^a = -38$
(3) $H_2 + Pt(111) \rightarrow 2H{-}Pt$	−85	−95	−90	$\Delta_{623K} = -90$
(4) $C_2H_6 + Pt(211) \rightarrow C_2H_5^{\ddagger}{-}Pt + 0.5H_2$	108	97	100	$\Delta_{623K} - 36^b = 64$
(5) $C_2H_6 + Pt(211) \rightarrow CHCH_3^{\ddagger}{-}Pt + H_2$	182	159	159	$\Delta_{623K} - 36^b = 123$
(6) $C_2H_6 + Pt(211) \rightarrow CHCH_2^{\ddagger}{-}Pt + 1.5H_2$	241	206	203	$\Delta_{623K} - 36^b = 167$

[a] 20 kJ/mol, an expected stabilization effect due to surface relaxation. A fixed parameter based on additional DFT calculations.[6] [b] 36 kJ/mol, a fitted parameter. A combined energetic effect due to surface relaxation, simplified (111) surface geometry used in the MC simulation, existence of more reactive sites than the model (211) surface.

and potential were described by the generalized gradient approximation (PW-91). The self-consistent PW-91 density was determined by iterative diagonalization of the Kohn−Sham Hamiltonian, Fermi population of the Kohn−Sham states (k_BT = 0.1 eV), and Pulay mixing of the resulting electronic density. All reported binding energies were extrapolated to $k_BT = 0$ eV.

State-of-the-art DFT slab calculations use 4 or more atomic layers, allowing the first one or two layers to relax during optimization to account for surface relaxation. In the present paper, we use results from 2-layer DFT calculations only to provide initial guesses for fitted model parameters and for identification of systematic trends caused by variations in surface coverages. Also, although effects of slab thickness and surface relaxation may be important for determining absolute values of binding energies from DFT calculations, these effects are less important for estimating lateral interaction parameters between adsorbed species (because these parameters are calculated from differences in binding energies). Our DFT calculations indicate that the combined effect of increasing the slab thickness to three layers and relaxing the first metal layer stabilizes hydrocarbon surface species by about 20 kJ/mol.[6] To compensate for the approximate nature of the current DFT calculations, a fixed stabilization parameter of 20 kJ/mol was incorporated explicitly into the adsorption energies used in the MC simulation for the stable hydrocarbon species: di-σ-bonded ethylene and ethylidyne, as shown in Table 1. The stabilization effect is also incorporated into the energies of formation of $C_2H_x^{\ddagger}$ hydrocarbon transition state complexes through a single adjustable parameter, which is discussed in detail in the section on MC parameters below.

Additional slab calculations were used to estimate ethylidyne−ethylidyne, ethylidyne−hydrogen, and hydrogen−hydrogen lateral interactions.[5] Briefly, two-layer fixed Pt(111) slabs with 2 × 2 and 2 × 3 unit cells were used with hydrocarbon species constrained in the $x-y$ plane parallel to the surface in positions identified as the most stable configurations on the clean Pt(111). Atomic hydrogen was constrained to the symmetric atop, bridge-bonded (2-fold) and 3-fold sites. The results of these coverage effect calculations are summarized in Figure 1.

In the present study, we complement the above DFT results with estimates for lateral interaction energies between atomic hydrogen and activated complexes, $C_2H_5^{\ddagger}$ and $CHCH_3^{\ddagger}$, for cleavage of the C−C bond in adsorbed C_2H_5 and $CHCH_3$ species. The considered surface arrangements on two-layer fixed Pt(111) slabs with 2 × 2 unit cells are presented in Figure 2. Only the top metal layer is shown in Figure 2 for clarity. Similar to our previous calculations, hydrocarbon species were constrained in the $x-y$ plane parallel to the surface in positions identified as the most stable configurations on the clean Pt(111) surface, and atomic hydrogen was constrained to the symmetric bridge-bonded and 3-fold sites. Estimates for lateral pairwise interaction energy changes on bringing species from

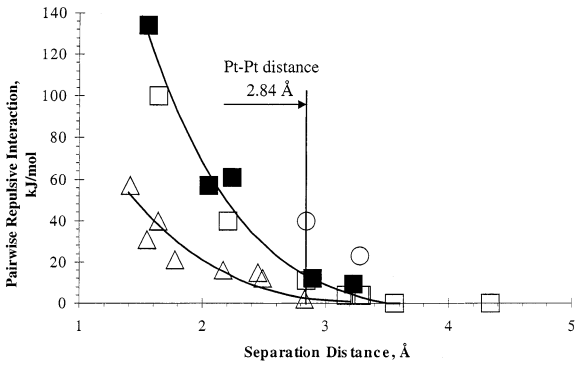

Figure 1. Pairwise repulsive interaction energy vs separation distance: (△) H−H; (□) C_2H_3−H; (■) $C_2H_x^{\ddagger}$−H; (○) $C_2H_3{-}C_2H_3$.

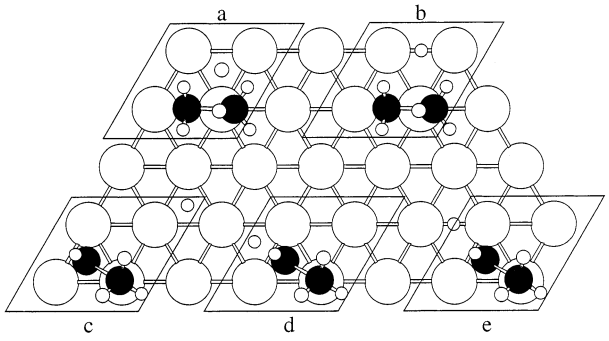

Figure 2. Model configurations used for estimating lateral interaction energies between atomic hydrogen and $C_2H_x^{\ddagger}$ species on Pt(111) with a 2 × 2 unit cell: (a, b) $C_2H_5^{\ddagger}$; (c−e) $CHCH_3^{\ddagger}$. Separation distances and energies are provided in Table 2.

infinite separation to neighboring positions were obtained by comparing binding energies with a quarter-monolayer coverage (one adsorbate per 2 × 2 unit cell) and with a hydrocarbon and hydrogen in the same unit cell in arrangements in Figure 2. The results of the calculations are summarized in Table 2.

All lateral interaction energies are repulsive. These repulsive interaction energies are shown in Figure 1 as a function of the separation distance between the centers of the neighboring hydrogen atom and the carbon atom closest to the surface (the one with fewer bonding hydrogens). Figure 1 also shows results from our previous DFT calculations of repulsive interaction energies between adsorbed hydrogen and ethylidyne species. We note that the lateral interaction energy is not expected to be a continuous function of the defined separation distance. The energy also depends on the orientation of the nonsymmetric hydrocarbon species, and on the symmetry of the hydrogen adsorption site. In addition, effects of surface relaxation, slab thickness, and unit cell size were not considered. Therefore, our results provide only a rough estimate for trends in lateral interaction energies, where each point is averaged over different configurations for a given separation distance.

TABLE 2: Estimates of Lateral Interaction Energies

surface arrangement (as shown in Figure 2)	C−H separation distance, Å	interaction energy, kJ/mol
(a) H−CH_2−CH_3	2.2	61
(b) H−CH_2−CH_3	2.9	12
(c) H−CH−CH_3	3.2	10
(d) H−CH−CH_3	1.6	134
(e) H−CH−CH_3	2.1	57

The trend line for the repulsive interactions between atomic hydrogen and the $C_2H_5^{\ddagger}$ and $CHCH_3^{\ddagger}$ transition states, shown in Figure 1, was fitted by a cubic polynomial:

$$\omega = -13.12r^3 + 139.16r^2 - 506.06r + 632.68 \qquad (3)$$

where ω is the repulsive pairwise interaction energy in kJ/mol and r is the separation distance in Å. The same equation describes the repulsive interaction energies between adsorbed hydrogen atoms and ethylidyne species, when the polynomial constant is decreased by 4 kJ/mol. The lower repulsion energies for the ethylidyne species are related to their more compact vertical geometry compared to the more parallel-lying transition states with extended C−C bond lengths. It is interesting to note that the sign and magnitude of the polynomial coefficients in eq 3 are similar to those estimated for lateral interactions between H, C_2H_5, and C_2H_4 on Pd(100) with extended Hückel calculations on metal clusters.[2]

4. Monte Carlo Simulation

4.1. Hydrogen and Ethane Coadsorption. Grandcanonical Monte Carlo (MC) simulations were used to calculate surface coverages of atomic hydrogen, di-σ-boned ethylene, and ethylidyne species, as a function of temperature and partial pressures of gas-phase ethane and molecular hydrogen. The MC simulation is based on our previously described model for CO adsorption and the coadsorption of hydrogen atoms and ethylidyne species on Pt(111).[5,48] Briefly, the simulation uses a two-dimensional 42 × 42 lattice with periodic boundary conditions. For each calculation, a temperature and partial pressures are specified. The chemical potentials of ethane and molecular hydrogen are determined by assuming an ideal-gas behavior for a given pressure and temperature. The temperature and chemical potential of the species in the gas phase are set equal to those of the corresponding surface species. Adsorption of molecular hydrogen produces two hydrogen atoms. Adsorption of ethane produces a di-σ-bonded ethylene species and two hydrogen atoms on the surface or an ethylidyne species and three surface hydrogen atoms.

The MC simulation uses three types of trial moves: particle insertion, removal, and position change (surface diffusion). On an insertion trial, the number and types of species on neighboring sites are analyzed for a randomly selected lattice site. The trial energy change is calculated by correcting the adsorption energy on an empty lattice with the appropriate lateral interaction for each of these adjacent species. The probability of accepting the adsorption move is then calculated on the basis of the energy change, partial pressure, and temperature in accordance with grandcanonical ensemble equations.[49] The acceptance of desorption and diffusion trial moves is evaluated in the same way. Because adsorption−desorption and diffusion under the simulation conditions are expected to be quasi-equilibrated, diffusion trials are modeled with jump moves; i.e., a particle can move from its original position to any suitable vacant site on the lattice. Similarly, on adsorption−desorption trials, particles are inserted and removed from randomly selected sites.

Surface species are restricted to high-symmetry sites: atop, bridge-bonded, and 3-fold sites. On the basis of our previously reported DFT results for the energetics of adsorption on different types of sites, atomic hydrogen is allowed to adsorb on any of these sites, and the adsorption of hydrocarbon species is restricted to their most favorable configurations on a clean surface: ethylidyne in 3-fold and di-σ-bonded ethylene in 2-fold (bridge) sites.[5,6] Because the energy changes for adsorption of ethylidyne species and hydrogen atoms were found in our DFT calculations to be similar on the 3-fold fcc and hcp sites, these 3-fold sites are not distinguished in our model.

4.2. Simulation of Hydrogenolysis Kinetics. As mentioned above, we model fast reaction steps, adsorption−desorption and hydrogenation-dehydrogenation, separately from the slow C−C bond breaking reactions. This separation of reaction steps into groups based on their relative rates reduces the number of simulation parameters: only the parameters describing the quasi-equilibrium for the fast reactions are required, instead of all factors affecting forward and reverse rate constants. In addition, such separation is beneficial because each reaction group can be treated with its own separate most numerically efficient algorithm. For a detailed molecular modeling of ethane hydrogenolysis, for example, the hydrogen−ethane coadsorption background, obtained with a grandcanonical ensemble, could be used with a kinetic molecular algorithm for C−C bond scission reactions based on rapidly developing dynamic MC methods.[1,2,50] Such an algorithm would include the formation and subsequent C−C bond breaking of reactive C_2H_x species on a lattice covered with hydrogen, di-σ-bonded ethylene, and ethylidyne.

A simplification in this algorithm can be made on the basis of the assumption of equilibration of the reactive C_2H_x species with the gas phase (eq 1). With this assumption, the concentrations of reactive species could be obtained through a grandcanonical algorithm. Only the cracking of these species would have to be described with a dynamic simulation. In our hydrogen-ethane coadsorption model, only the most stable, and thus, most abundant surface species, are considered. In particular, π-bonded ethylene species, which are less stable than the di-σ-bonded ethylene, are not considered because their concentration is expected to be negligible at typical hydrogenolysis reaction conditions.[6,16,40] Therefore, it is consistent to neglect the effect of the presence of the reactive C_2H_x species on the thermodynamic state of the surface. In this case, it is only necessary to evaluate the dependence of the concentrations of the reactive C_2H_x species on the hydrogen-di-σ-ethylene-ethylidyne coadsorption background.

A further simplification to the reactivity model can be made on the basis of the equilibration of the reactive C_2H_x species and their corresponding transition states $C_2H_x^{\ddagger}$. According to the transition state theory, the active species are in quasi-equilibrium with the corresponding transition states for the cleavage of the C−C bond, and the rate of ethane hydrogenolysis can be described by the sum of coverage values for each transition state times a frequency factor: $r = (kT/h)\sum\theta_{C_2H_x^{\ddagger}}$. Because the active C_2H_x species are in quasi-equilibrium with

gaseous ethane and hydrogen, the transition states may also be treated as being in equilibrium with the gas phase. As a result, the stable C_2H_x species leading to the formation of the $C_2H_x^{\ddagger}$ transition state complexes can be excluded from the simulation. To summarize, the hydrogenolysis reaction rate can be modeled by simulating concentrations of the $C_2H_x^{\ddagger}$ transition state complexes in equilibrium with gas-phase ethane and hydrogen as a function of the state of the catalytic surface covered with hydrogen, di-σ-ethylene, and ethylidyne species.

With this model formulation, it is numerically efficient to simulate equilibrated $C_2H_x^{\ddagger}$ concentrations with a grandcanonical ensemble, using a "virtual insertion" method. This method is primarily used in NVT ensembles for calculating chemical potentials. The algorithm involves an attempt to insert a particle and the evaluation of the probability for this trial. The insertion is "virtual", because the trial is never accepted. In our grandcanonical simulation, we use virtual insertion to compute configurational probabilities of simultaneously forming a $C_2H_x^{\ddagger}$ activated complex and $(6 - x)$ hydrogen atoms. A random empty site is selected for $C_2H_x^{\ddagger}$ adsorption, and the energy change is calculated. Subsequently, the site vacancies are reevaluated because the inserted hydrocarbon might have blocked neighboring sites, making them inaccessible for hydrogen. Then, $(6 - x)$ hydrogen atoms are inserted in random vacant sites, and the total energy change for the insertion of the hydrocarbon and the hydrogen atoms is computed. Finally, all the inserted species are removed and the probability of insertion is calculated from the following equation:

$$P = \left[1; \frac{N_{\text{empty-HC-TS}} N_{\text{empty-H}} (N_{\text{empty-H}} - 1) \cdots (N_{\text{empty-H}} - (5 - x))}{(N_H + 1)(N_H + 2) \cdots (N_H + (6 - x))} \times \exp(\beta \mu_{C_2H_6} - \beta \Delta U) \right] \quad (4)$$

where $N_{\text{empty-HC-TS}}$ is the number of empty sites available for the hydrocarbon transition state, $N_{\text{empty-H}}$ is the number of sites available for H adsorption after insertion of $C_2H_x^{\ddagger}$, N_H is the number of hydrogen atoms on the surface, $\beta = 1/kT$, $\mu_{C_2H_6}$ is the chemical potential of gas-phase ethane, and ΔU is the potential energy change for the formation of $C_2H_x^{\ddagger}$ and $(6 - x)$ hydrogen atoms from ethane. The trial energy change ΔU is computed by reducing the energy of adsorption of $C_2H_x^{\ddagger}$ and $(6 - x)$H at infinite separation on a clean surface by the sum of repulsive interactions for each inserted surface particle. This energy change can be represented by the following thermodynamic cycle: adsorption of the transition state complex on the clean Pt surface with the production of the appropriate number of gas-phase hydrogen molecules (eq 5), transfer of the hydrocarbon complex from the clean lattice onto the simulated catalytic surface (eq 6), and adsorption of the formed hydrogen onto the simulated surface (eq 7):

$$\Delta U_{\text{HC-TS}}: \quad C_2H_6 + \text{Pt(clean)} \rightarrow C_2H_x^{\ddagger}\text{-Pt(clean)} + \left(\frac{6 - x}{2}\right)H_2 \quad (5)$$

$$\omega_{\text{HC-TS}}: \quad C_2H_x^{\ddagger}\text{-Pt(clean)} \rightarrow C_2H_x^{\ddagger}\text{-Pt(covered)} \quad (6)$$

$$\sum_{6-x} \Delta H_U: \quad \left(\frac{6 - x}{2}\right)H_2 + \text{Pt(clean)} \rightarrow (6 - x)\text{H-Pt(covered)} \quad (7)$$

The energy change, therefore, can be written as the following sum:

$$\Delta U = \Delta U_{\text{HC-TS}} + \omega_{\text{HC-TS}} + \sum_{6-x} \Delta U_H \quad (8)$$

Equation 4 for the probability of the virtual insertion trial can be written as the product of the trial probability when the energy change for the formation of $C_2H_x^{\ddagger}$ on the clean Pt surface with the liberation of gas-phase hydrogen is zero, multiplied by the exponential factor correcting for a nonzero value:

$$P = P(\Delta U_{\text{HC-TS}} = 0) \exp(-\beta \Delta U_{\text{HC-TS}}) \quad (9)$$

The above separation of the contribution from the first reaction in the thermodynamic cycle (eq 5) is possible because the insertion trial is virtual and because the effect of all $C_2H_x^{\ddagger}$ transition states on the thermodynamic state of the lattice can be neglected due to their negligibly low coverages. Surface concentrations of the transition state complexes are calculated by assuming that the average probability of virtual insertion trials for a particular $C_2H_x^{\ddagger}$ species equals the probability of finding a single species of this type on our lattice. Consequently, the coverage values for the hydrocarbon transition states have the following form:

$$\theta = \theta(\Delta U_{\text{HC-TS}} = 0) \exp(-\beta \Delta U_{\text{HC-TS}}) \quad (10)$$

We first use the MC simulation to calculate coverage values for the transition states as a function of partial pressures, temperature, and hydrogen adsorption and lateral interactions energies. We then correct these values by the exponential factor with the appropriate energy change for the formation of the transition state from ethane. This algorithm eliminates the numerical problem of handling small probability numbers within the simulation. In this sense, it is similar to a standard normalization method. However, a more important benefit of this approach is the independence of the initial simulation results from the adsorption energies of the transition state species. For these species, the simulation provides coverage information based on only their geometries and lateral interactions, and it is not necessary to re-run numerically expensive simulations if adsorption energetics need to be updated or fitted to experimental results.

4.3. Simulation Parameters. The parameters of the MC simulation are adsorption energies for hydrogen atoms, di-σ-bonded ethylene, ethylidyne and three different $C_2H_x^{\ddagger}$ activated complexes on a clean Pt surface. The adsorption energies shown in Table 1 are adjusted to 623 K (a typical temperature for ethane hydrogenolysis over Pt) by adding zero-point energy and temperature corrections obtained through frequency calculations.[6] Pairwise lateral interactions were used as additional simulation parameters. These interactions determine adjustments to the adsorption energies based on the type and number of neighboring surface species for each adsorbed particle. The total rate of ethane hydrogenolysis is computed as the sum of coverages for each $C_2H_x^{\ddagger}$ transition state times a frequency factor:

$$r = \frac{kT}{h}(\theta_{C_2H_5^{\ddagger}} + \theta_{CH-CH_3^{\ddagger}} + \theta_{CH-CH_2^{\ddagger}}) \quad (11)$$

We have shown elsewhere[5] that the simulation parameters in Table 1 for hydrogen adsorption on Pt(111) adequately describe the experimental dependence of the heat of adsorption on coverage at 300−673 K. However, a challenge of selecting

a model surface for hydrogenolysis reactions on metals is the structure sensitivity of these reactions. The C−C bond scission is thought to proceed through hydrocarbon species adsorbed on highly uncoordinated surface metal sites.[7,16] For example, results from DFT calculations show lower activation barriers for C−C bond cleavage on coordinatively unsaturated sites on Pt(211) sites compared to terrace sites on Pt(111).[6] Accordingly, we have employed hydrocarbon adsorption energies calculated using the Pt(211) model surface as values for the simulation parameters in the present study.

A simplification to the MC model can be made by assuming that the energetic effects due to the geometric differences between the (211) and (111) planes are small compared to the uncertainties in the DFT estimates of the activation barriers. We tested this assumption by running simulations on a (211) model surface and comparing the results to those obtained on a (111) plane using (211) energetics for the hydrocarbon species. The comparison indicates that changes in the structure of neighboring sites lead to variations in the apparent adsorption energy changes of less than 10 kJ/mol. As a result, the incorporation of the adjustable stabilization parameter for the transition state complexes, which is expected to be at least 20 kJ/mol from DFT calculations, justifies the use of a simplified (111) geometry in the MC model with energetic parameters derived from DFT calculations on Pt(211).

The simulation uses first-, second-, and third-neighbor lateral interaction energies for hydrogen−hydrogen, hydrogen−ethylidyne, and ethylidyne−ethylidyne pairs reported previously.[5] The summary of the interaction energies as a function of the separation distance is provided in Figure 1. It is assumed that hydrogen−hydrocarbon and hydrocarbon−hydrocarbon interaction energies are similar for ethylidyne and di-σ-bonded ethylene species. Consequently, the simulation uses the same interaction energies for both stable hydrocarbon species. For the di-σ-bonded ethylene, the separation distance is measured from the center of the C−C bond. For the $C_2H_x^{\ddagger}$ transition state complexes, the simulation uses the regression eq 3 to describe the lateral interactions with hydrogen. All neighboring interactions between the $C_2H_x^{\ddagger}$ transition states and the stable hydrocarbon species are assumed to be similar to ethylidyne−ethylidyne interaction energies shown in Figure 1. A value of 40 kJ/mol was used for the second-neighbor ethylidyne−ethylidyne interaction energy for all geometries with separation distances between 2.5 and 3 Å. For surface arrangements with separation distances between 3 and 4 Å, the value for the third-neighbor ethylidyne−ethylidyne interaction of 23 kJ/mol was used. Thus, different fits/values are used for the distinct lateral interaction energies.

The simulation data indicate that varying the interaction energies between $C_2H_x^{\ddagger}$ and the stable hydrocarbons by ±10 kJ/mol has a negligible effect on the model results. This insensitivity can be attributed to two separate factors. First, the simulation predicts that the surface is primarily covered by hydrogen under the usual reaction conditions, as shown in Figure 4a−d. Therefore, the hydrocarbon−hydrocarbon interactions in general are not as critical as the hydrogen−hydrogen and hydrogen−hydrocarbon interactions under the studied conditions. Second, the hydrocarbon−hydrocarbon interactions are larger than the hydrogen−hydrocarbon interactions. These large repulsive interactions make it highly unlikely for two hydrocarbon species to be in neighboring sites if other adsorption sites are available. Therefore, small variations in the absolute repulsion values do not modify the energetics of neighboring sites but result in the same apparent geometric blocking.

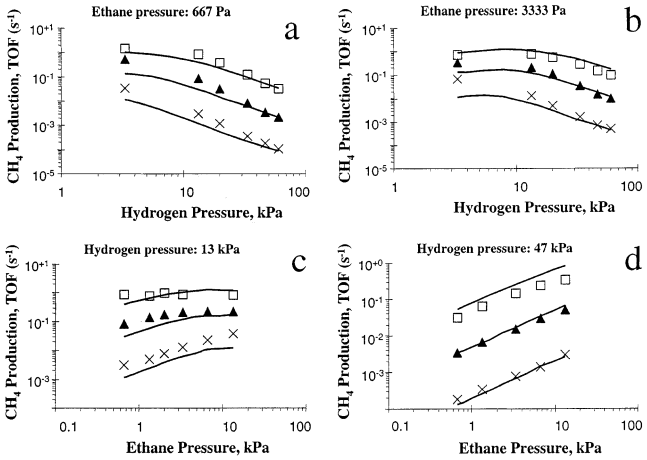

Figure 3. Rate of methane production, TOF (s^{-1}): (□) 673 K; (▲) 623 K; (×) 573 K; (solid line) MC simulation.

In the sampling algorithm, adsorption, desorption, and diffusion trials for the stable species were generated with equal probability to reach system equilibration. After equilibration, virtual insertion trials were added. The following sampling ratios were then used to facilitate convergence: 0.1 for random stable species moves, and 0.2, 0.2, and 0.5 for $C_2H_5^{\ddagger}$, $CHCH_3^{\ddagger}$, $CHCH_2^{\ddagger}$ virtual insertions, correspondingly. Fluctuations in the values of the lattice coverage and total energy were monitored to determine simulation convergence.[48] A typical number of trials to reach equilibration was $(0.1-1) \times 10^6$. Simulation results were obtained by discarding the first 4×10^6 trial moves to allow the system to equilibrate and then averaging coverage and energy values for the next 4×10^7 trial moves.

5. Results and Discussion

Results of MC simulations for the rate of methane production from ethane hydrogenolysis are presented in Figure 3. These results were obtained by adjusting the stabilization parameter for the $C_2H_x^{\ddagger}$ transition states to a value of 36 kJ/mol, in an effort to fit the experimental data[16] for ethane hydrogenolysis over a Pt/SiO_2 catalyst. It can be seen that the MC simulation model is, in fact, able to describe the main trends in the experimental data by adjusting this single model parameter.

The predictions of the MC simulation are presented in Figure 4a−d for the surface coverages by hydrogen, ethylidyne, and di-σ-bonded ethylene at 623 K. The model predicts that the catalytic surface is primarily covered by atomic hydrogen and ethylidyne species. This prediction is consistent with the NMR experimental evidence, which suggests that the most abundant hydrocarbon species have a C_2H_3 stoichiometry.[17] In addition, the adsorption of the di-σ-bonded ethylene species appears to be important in modeling ethane hydrogenolysis. In particular, the simulation indicates that the coverage of di-σ-bonded ethylene is lower than that of ethylidyne species only when both ethane and hydrogen partial pressures are low (Figure 4a,b).

The results from MC simulations for the surface concentrations of the three $C_2H_x^{\ddagger}$ transition states at 623 K are presented in Figure 4e−h. The surface concentration of the $C_2H_5^{\ddagger}$ transition state is about 1 order of magnitude higher than the concentrations of the $CHCH_3^{\ddagger}$ and $CHCH_2^{\ddagger}$ transition states. Accordingly, about 80% of the overall hydrogenolysis rate can be attributed to the reactivity of the $C_2H_5^{\ddagger}$ transition state. This conclusion is consistent with our previous ethane hydrogenolysis kinetic models, which suggest that the catalytic surface is primarily covered by the spectator CCH_3 ethylidyne species,

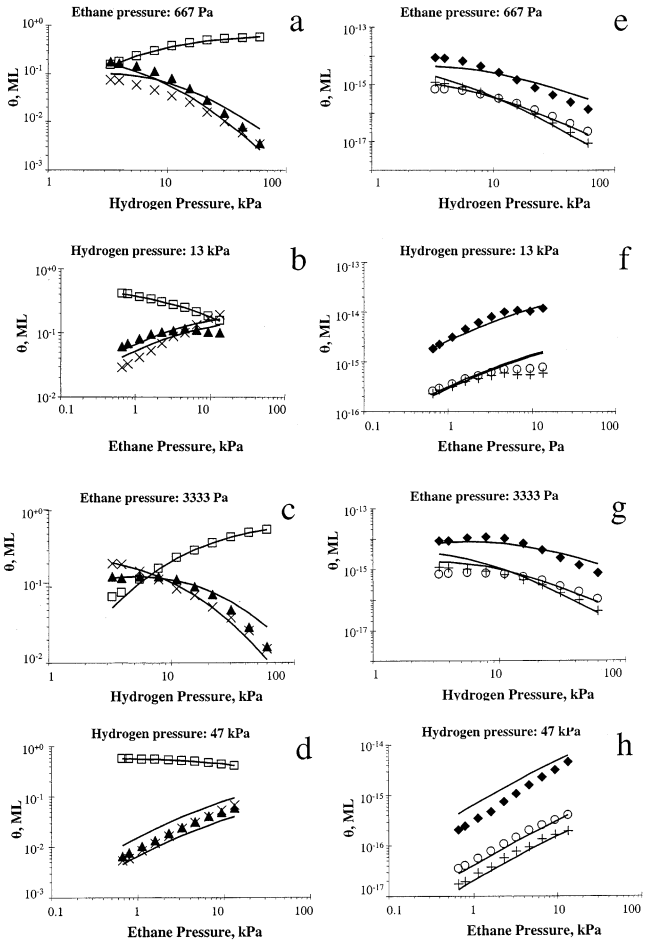

Figure 4. Surface concentrations of stable species (a−d) and $C_2H_x^{\ddagger}$ transition state complexes (e−h) predicted by the MC simulation at 623 K: (a−d) (□) H, (▲) CCH_3 ethylidyne, (×) CH_2CH_2 di-σ-bonded ethylene; (e−h) (◆) $C_2H_5^{\ddagger}$, (+) $CHCH_3^{\ddagger}$, (○) $CHCH_2^{\ddagger}$. Solid lines: empirical isotherm equations (19) and (20).

whereas the reactions proceed through more highly hydrogenated C_2H_x species.[7,16]

An important advantage of developing a molecular model for simulating reaction rates is the ability to utilize energetic information about stable and reactive species on a clean surface and then adjust these energetics within the simulation to correct for coverage effects. Lateral interactions become particularly important for modeling reactions over a wide range of experimental conditions, where the surface thermodynamics are expected to change significantly with coverage. For example, the simulation results of the current study suggest that the state of the surface changes from being primarily hydrogen-covered at most experimental conditions (Figure 4a−d) to being highly hydrocarbon-covered at low hydrogen partial pressures (Figure 4a,c). Yet, despite the large variation in surface coverage, the molecular model may describe the reaction kinetics with a single parameter being adjusted from its initial DFT estimate.

An important aspect of using lateral interactions to describe coverage-dependent energetics is the ability to predict changes in apparent kinetic reaction orders with respect to changes in reaction conditions. For example, the most negative apparent hydrogen order dependence for the ethylidyne surface coverage with coverage-independent energetics using reaction eq 1 is −2.0. However, this order decreases to −2.2 if interactions between adsorbed hydrogen atoms and ethylidyne species are taken into account.[5] Importantly, higher repulsive interactions lead to more negative apparent reaction orders with respect to hydrogen pressure. Specifically, if the lateral interactions between the $C_2H_5^{\ddagger}$ transition states complexes and atomic hydrogen, described by eq 3, are decreased by 4 kJ/mol, the apparent hydrogen pressure orders in the high hydrogen pressure region at 623 K would change from about −1.8 (Figure 3a,b) to −1.1 and −0.9 at ethane partial pressures of 667 and 3333 kPa, correspondingly. Furthermore, the model would predict reaction rates that are up to 20 times higher than the presented results. Therefore, the lateral interaction energies in the current model significantly influence both kinetic trends and absolute reaction values.

The results from the DFT calculations of this study are not sufficiently accurate to make first-principles predictions of the rate of ethane hydrogenolysis over Pt (e.g., two-layer slabs, neglect of surface relaxation). Thus, it is useful to develop an empirical description of MC simulation results of the present study, with an aim of describing how the trends displayed by the surface coverages by stable adsorbed species and transition states are influenced by the values of the surface interaction parameters (estimated by DFT calculations). This empirical model could then be used to predict the state of the surface and the rate of ethane hydrogenolysis for different values of the surface interaction parameters (calculated from more accurate DFT calculations). Such an empirical description can be obtained by considering the following quasi-equilibrated reactions:

$$H_2 + 2* \rightleftarrows 2H* \tag{12}$$

$$C_2H_6 + * \rightleftarrows CCH_3* + {}^3/_2H_2 \tag{13}$$

$$C_2H_6 + * \rightleftarrows CH_2CH_2* + H_2 \tag{14}$$

$$C_2H_6 + * \rightleftarrows CH_2CH_3^{\ddagger}* + {}^1/_2H_2 \tag{15}$$

$$C_2H_6 + * \rightleftarrows CHCH_3^{\ddagger}* + H_2 \tag{16}$$

$$C_2H_6 + * \rightleftarrows CHCH_2^{\ddagger}* + {}^3/_2H_2 \tag{17}$$

$$1 = \theta_* + \theta_H + 2\theta_{CH_2CH_2} + 3\theta_{CCH_3} \tag{18}$$

This model assumes that surface hydrogen, di-σ-bonded ethylene, and ethylidyne block 1, 2, and 3 sites, respectively; and surface concentrations of transition state species are neglected in the site balance equation (18).

Surface concentrations for hydrogen and hydrocarbon species can be expressed in the following form:

$$\theta_H = \sqrt{K_H P_{H_2}}\,\theta \tag{19}$$

$$\theta_{C_2H_x} = K_{C_2H_x} P_E P_{H_2}^{(x-6)/2} \theta_* \tag{20}$$

where K_i are equilibrium adsorption constants and P_{H_2} and P_E are hydrogen and ethane partial pressures. The ratio of vacant sites is then given by

$$\theta_* = \frac{P_{H_2}^{1.5}}{\sqrt{K_H} P_{H_2}^{2} + 3K_{CCH_3} P_E + 2K_{CH_2CH_2} P_E P_{H_2}^{0.5} + P_{H_2}^{1.5}} \tag{21}$$

TABLE 3: Enthalpy and Entropy Values for Empirical Coadsorption Equations (19)−(24) at 623 K

species	ΔH, kJ/mol	ΔS, J/(mol K)
H*	−92	−90 ± 10
CCH_3*	−5	38 ± 13
C_2H_4 (di-σ)*	−38	−5 ± 13
$C_2H_5^{\ddagger}$*	63	−81 ± 13
$CHCH_3^{\ddagger}$*	123	−11 ± 14
$CHCH_2^{\ddagger}$*	168	52 ± 14

TABLE 4: Lateral Interaction Parameters for Empirical Coadsorption Equations (22)−(24)

parameter	kJ/mol
ω_{HH}	49 ± 11
ω_{HC-H}	53 ± 14
$\omega_{HC(TS)-H}$	70 ± 16
ω_{HC-HC}	85 ± 22

The effect of lateral interactions can be incorporated into the model using the following dependence of the equilibrium constants on surface coverage:

$$K_H = \exp\left(-\frac{\Delta H_H}{RT} + \frac{\Delta S_H}{R}\right) \times \exp\left(-\frac{\omega_{HH}\theta_H + \omega_{HC-H}(\theta_{CCH_3} + \theta_{CH_2CH_2})}{RT}\right) \quad (22)$$

$$K_{HC} = \exp\left(-\frac{\Delta H_{HC}}{RT} + \frac{\Delta S_{HC}}{R}\right) \times \exp\left(-\frac{\omega_{HC-H}\theta_H + \omega_{HC-HC}(\theta_{CCH_3} + \theta_{CH_2CH_2})}{RT}\right) \quad (23)$$

$$K_{HC(TS)} = \exp\left(-\frac{\Delta H_{HC(TS)}}{RT} + \frac{\Delta S_{HC(TS)}}{R}\right) \times \exp\left(-\frac{\omega_{HC(TS)-H}\theta_H + \omega_{HC-HC}(\theta_{CCH_3} + \theta_{CH_2CH_2})}{RT}\right) \quad (24)$$

In these equations, K_H, K_{HC}, and $K_{HC(TS)}$ are equilibrium constants for adsorption of hydrogen, stable hydrocarbon species, and transition state complexes, respectively, and ω_{HH}, ω_{HC-H}, $\omega_{HC(TS)-H}$, and ω_{HC-HC} are parameters representing energies of hydrogen−hydrogen, hydrocarbon−hydrogen, hydrocarbon (transition state species)−hydrogen, and hydrocarbon−hydrocarbon lateral interactions, respectively.

Enthalpy changes were calculated on the basis of adsorption energies in Table 1. Entropy changes and lateral interaction parameters were fitted with Athena Visual Workbench 4.1 nonlinear regression software, Stewart & Associates, Madison, WI. Model parameters with 95% confidence intervals for fitted values are presented in Tables 3 and 4. We note that the fitted entropy changes are similar for hydrocarbon species having the same stoichiometry. In addition, values for repulsive interaction parameters increase in the following sequence: hydrogen−hydrogen, hydrogen−stable hydrocarbon, hydrogen−TS, hydrocarbon−hydrocarbon. Importantly, the values of the fitted parameters are in agreement with values reported previously for a H−CCH_3 coadsorption model.[5] Surface coverage values obtained with eqs 19 and 20 are shown as solid lines in Figure 4. Differences between these results and MC simulation data are due to the mean-field approximation in treating the coverage effects in the empirical model.

6. Conclusions

A grandcanonical Monte Carlo simulation was used to predict the quasi-equilibrated concentrations of the most abundant surface species adsorbed on Pt(111) under ethane hydrogenolysis reaction conditions, i.e., adsorbed atomic hydrogen, ethylidyne species (CCH_3), and di-σ-bonded ethylene. The MC simulation results of the quasi-equilibrated adsorption steps were used as a background for modeling the rate of ethane hydrogenolysis, based on the surface concentrations of $C_2H_x^{\ddagger}$ transition states involved in C−C bond scission reactions. The surface coverage values for $C_2H_x^{\ddagger}$ transition states were estimated with a MC "virtual insertion" sampling algorithm using energetics reported for coordinatively unsaturated sites on Pt(211).[6] The model successfully describes experimental data for the rate of ethane hydrogenolysis for a Pt/SiO_2 catalyst over a wide range of conditions: $P_{H_2} = 3-60$ kPa, $P_{C_2H_6} = 0.7-13$ kPa, 573−673 K.

The parameters of the MC simulation are energy changes for adsorption of surface species and pairwise lateral interaction energies between these species. All estimates for simulation parameters were obtained from density functional theory calculations. In particular, the energetics of hydrogen atoms, ethylidyne species, di-σ-bonded ethylene, and three most stable $C_2H_x^{\ddagger}$ transition state species ($C_2H_5^{\ddagger}$, $CHCH_3^{\ddagger}$, and $CHCH_2^{\ddagger}$) reported earlier[5,6] were complemented with new DFT results for the lateral interaction energies between $C_2H_x^{\ddagger}$ and H species. A fitted polynomial equation is reported for the lateral interaction energy between adsorbed $C_2H_x^{\ddagger}$ and H species versus the distance between these species. The simulation shows that larger repulsive interactions between $C_2H_x^{\ddagger}$ and H species lead to more negative reaction orders with respect to the hydrogen pressure.

The MC simulation results can be described by empirical equations for equilibrated adsorption isotherms, incorporating an explicit dependence of the equilibrium constants on surface coverage. Equilibrium constants for adsorption were expressed in terms of enthalpy and entropy changes, as well as lateral interaction energies. The enthalpy changes for the empirical adsorption model were obtained from DFT calculations results. Values for entropy changes and repulsive interaction energies were obtained by fitting the MC results with the empirical model, and these values are in agreement with parameters reported previously for a H−CCH_3 coadsorption model.[5] The state of the Pt surface is predicted to change from being primarily hydrogen-covered at most experimental conditions to being highly hydrocarbon-covered at low hydrogen partial pressures. Pairwise lateral interaction energies were found useful for incorporating surface coverage effects in the reaction rate model to account for large variations in the state of the catalyst for a wide range of reaction conditions.

Acknowledgment. Acknowledgment is made to the donors of the Petroleum Research Fund, administered by the American Chemical Society, for support of this research.

References and Notes

(1) Jansen, A. P. J.; Lukkien, J. J. *Catal. Today* **1999**, *53*, 259.
(2) Hansen, E. W.; Neurock, M. *Chem. Eng. Sci.* **1999**, *54*, 3411.
(3) Duca, D.; La Manna, G.; Russo, M. R. *Phys. Chem. Chem. Phys.* **1999**, *1*, 1375.
(4) Duca, D.; Barone, G.; Varga, Z. *Catal. Lett.* **2001**, *72*, 17.
(5) Podkolzin, S. G.; Watwe, R. M.; Yan, Q.; de Pablo, J. J.; Dumesic, J. A. *J. Phys. Chem. B* **2001**, *105*, 8550.
(6) Watwe, R. M.; Cortright, R. D.; Norskov, J. K.; Dumesic, J. A. *J. Phys. Chem. B* **2000**, *104*, 2299.
(7) Cortright, R. D.; Watwe, R. M.; Spiewak, B. E.; Dumesic, J. A. *Catal. Today* **1999**, *53*, 395.
(8) Sinfelt, J. H. *J. Catal.* **1972**, *27*, 468.
(9) Sinfelt, J. H. *Adv. Catal.* **1973**, *23*, 91.
(10) Gudkov, B. S.; Guczi, L.; Tetenyi, P. *J. Catal.* **1982**, *74*, 207.

(11) Zaera, F.; Somorjai, G. A. *J. Phys. Chem.* **1985**, *89*, 3211.
(12) Zaera, F.; Janssens, T. V. W.; Ofner, H. *Surf. Sci.* **1996**, *368*, 371.
(13) Janssens, T. V. W.; Stone, D.; Hemminger, J. C.; Zaera, F. *J. Catal.* **1998**, *177*, 284.
(14) Rekoske, J. E.; Cortright, R. D.; Goddard, S. A.; Sharma, S. B.; Dumesic, J. A. *J. Phys. Chem.* **1992**, *96*, 1880.
(15) Cimino, A.; Boudart, M.; Taylor, H. S. *J. Phys. Chem.* **1954**, *58*, 796.
(16) Cortright, R. D.; Watwe, R. M.; Dumesic, J. A. *J. Mol. Catal. A—Chem.* **2000**, *163*, 91.
(17) Klug, C. A.; Slichter, C. P.; Sinfelt, J. H. *J. Phys. Chem.* **1991**, *95*, 2119.
(18) Nieuwenhhuys, B. E. *Surf. Sci.* **1976**, *59*, 430.
(19) Norton, P. R.; Davies, J. A.; Jackman, T. E. *Surf. Sci.* **1982**, *121*, 1013.
(20) Christmann, K.; Ertl, G.; Pignet, T. *Surf. Sci.* **1976**, *54*, 365.
(21) Lu, K. E.; Rye, R. R. *Surf. Sci.* **1974**, *45*, 677.
(22) Lee, J.; Cowin, J. P.; Wharton, L. *Surf. Sci.* **1983**, *130*, 1.
(23) McCabe, R. W.; Schmidt, L. D. *Surf. Sci.* **1977**, *65*, 189.
(24) Poelsema, B.; Mechtersheimer, G.; Comsa, G. *Surf. Sci.* **1981**, *111*, 519.
(25) Koeleman, B. J. J.; de Zwart, S. T.; Boers, A. L.; Poelsema, B.; Verhey, L. K. *Nucl. Instrum. Methods Phys. Res.* **1983**, *218*, 225.
(26) Cerny, S.; Smutek, M.; Buzek, F. *J. Catal.* **1975**, *38*, 245.
(27) Norton, P. R.; Richards, P. J. *Surf. Sci.* **1974**, *44*, 129.
(28) Lantz, J. B.; Gonzalez, R. D. *J. Catal.* **1976**, *41*, 293.
(29) NatalSantiago, M. A.; Podkolzin, S. G.; Cortright, R. D.; Dumesic, J. A. *Catal. Lett.* **1997**, *45*, 155.
(30) Sen, B.; Vannice, M. A. *J. Catal.* **1991**, *130*, 9.
(31) Olsen, R. A.; Kroes, G. J.; Baerends, E. J. *J. Chem. Phys.* **1999**, *111*, 11155.
(32) Watson, G. W.; Wells, R. P. K.; Willock, D. J.; Hutchings, G. J. *Chem. Commun.* **2000**, *8*, 705.
(33) Papoian, G.; Norskov, J. K.; Hoffmann, R. *J. Am. Chem. Soc.* **2000**, *122*, 4129.
(34) De La Cruz, C.; Sheppard, N. *Phys. Chem. Chem. Phys.* **1999**, *1*, 329.
(35) De La Cruz, C.; Sheppard, N. *J. Catal.* **1991**, *127*, 445.
(36) Beebe, T. P.; Yates, J. T. *J. Am. Chem. Soc.* **1986**, *108*, 663.
(37) Starke, U.; Barbieri, A.; Materer, N.; Vanhove, M. A.; Somorjai, G. A. *Surf. Sci.* **1993**, *286*, 1.
(38) Steininger, H.; Ibach, H.; Lehwald, S. *Surf. Sci.* **1982**, *117*, 685.
(39) Sheppard, N.; De La Cruz, C. *Adv. Catal.* **1996**, *41*, 1.
(40) Shen, J. Y.; Hill, J. M.; Watwe, R. M.; Spiewak, B. E.; Dumesic, J. A. *J. Phys. Chem. B* **1999**, *103*, 3923.
(41) Sheppard, N. *J. Electron Spectrosc. Relat. Phenom.* **1986**, *38*, 175.
(42) Yeo, Y. Y.; Stuck, A.; Wartnaby, C. E.; King, D. A. *Chemical Physics Lett.* **1996**, *259*, 28.
(43) Palfi, S.; Lisowski, W.; Smutek, M.; Cerny, S. *J. Catal.* **1984**, *88*, 300.
(44) Spiewak, B. E.; Cortright, R. D.; Dumesic, J. A. *J. Catal.* **1998**, *176*, 405.
(45) Stuck, A.; Wartnaby, C. E.; Yeo, Y. Y.; King, D. A. *Phys. Rev. Lett.* **1995**, *74*, 578.
(46) Nomikou, Z.; Van Hove, M. A.; Somorjai, G. A. *Langmuir* **1996**, *12*, 1251.
(47) Ge, Q.; King, D. A. *J. Chem. Phys.* **1999**, *110*, 4699.
(48) Podkolzin, S. G.; Shen, J. Y.; de Pablo, J. J.; Dumesic, J. A. *J. Phys. Chem. B* **2000**, *104*, 4169.
(49) Frenkel, D. Advanced Monte Carlo Techniques. In *Computer Simulation In Chemical Physics*; Allen, M. P., Tildesley, D. J., Eds.; Kluwer Academic Publishers: Dordrecht, Boston, 1993; Vol. 397, p 93.
(50) Lukkien, J. J.; Segers, J. P. L.; Hilbers, P. A. J.; Gelten, R. J.; Jansen, A. P. J. *Phys. Rev. E* **1998**, *58*, 2598.